

In situ dehydration of yugawaralite

GILBERTO ARTIOLI,^{1,*} KENNY STÅHL,² GIUSEPPE CRUCIANI,³ ALESSANDRO GUALTIERI,⁴ AND JONATHAN C. HANSON⁵

¹Dipartimento di Scienze della Terra, Università di Milano, I-20133 Milano, Italy
and CNR, Centro di Studio per la Geodinamica Alpina e Quaternaria, I-20133 Milano, Italy

²Chemistry Department, Danish Technical University, DK-2800 Lyngby, Denmark

³Istituto di Mineralogia, Università di Ferrara, I-44100 Modena, Italy

⁴Dipartimento di Scienze della Terra, Università di Modena e Reggio, I-41100 Modena, Italy

⁵Chemistry Department, Brookhaven National Laboratory, Upton, NY 11973, U.S.A.

ABSTRACT

The structural response of the natural zeolite yugawaralite ($\text{CaAl}_2\text{Si}_6\text{O}_{16}\cdot 4\text{H}_2\text{O}$) upon thermally induced dehydration has been studied by Rietveld analysis of temperature-resolved powder diffraction data collected *in situ* in the temperature range 315–791 K using synchrotron radiation. The room-temperature monoclinic structure [Pc , $a = 6.73200(9)$, $b = 14.0157(2)$, $c = 10.0607(1)$ Å, $\beta = 111.189(1)^\circ$, $Z = 2$, at 315 K] has the Ca cations in the channels coordinated to four framework O atoms and to four water molecules, with two of the water sites (OW1 and OW4) showing positional disorder progressively disappearing as the dehydration proceeds. The yugawaralite structure reacts to the release of water molecules with small changes in the Ca-O bond distances and minor distortions of the tetrahedral framework up to about 695 K. Above this temperature the Ca coordination falls below 7 (four framework O atoms and three water molecules) and a major rearrangement in the cation coordination takes place, causing a first order phase transition involving both a large decrease in the cell volume and the change in the space group symmetry. A satisfactory structure model for the high-temperature phase stable in the range 695–791 K could not be obtained because of the complexity of the structure. A model approximately describing the average structure [Pn , $a = 12.703(1)$, $b = 13.067(1)$, $c = 9.839(1)$ Å, $\beta = 110.894(9)$, $Z = 4$, at 749 K] has been used to follow the temperature evolution of the cell parameters in the measured temperature range. This model involves a sixfold coordination of the Ca cations (five framework O atoms and one water molecule). There is no indication of significant structure changes before collapse, likely occurring when the last water molecule is expelled from the structure and the cation coordination drops below 6, as observed in other Ca-rich zeolites (i.e., laumontite, scolecite, mesolite).

INTRODUCTION

Yugawaralite (ideally $\text{CaAl}_2\text{Si}_6\text{O}_{16}\cdot 4\text{H}_2\text{O}$) is a rare natural zeolite reported from a few occurrences in Alaska, Canada, Iceland, India, Italy, Japan, New Zealand, and Wyoming (see Gottardi and Galli 1985; Tschernich 1992 for reviews). The crystal structure was determined by X-ray single crystal diffraction (Kerr and Williams 1967, 1969; Laimer and Slaughter 1969) and subsequently refined by neutron single crystal diffraction at low temperature (Kvick et al. 1986). Yugawaralite has a peculiar topology composed by 5- and 4-membered rings of tetrahedra (YUG code, Meier et al. 1996) and a fully ordered distribution of aluminum atoms in the framework.

The dehydration behavior of yugawaralite was studied by *ex situ* thermogravimetry in air (Eberlein et al. 1971) and by X-ray single crystal diffraction in vacuum (Alberti et al. 1994, 1996). Eberlein and coworkers reported the loss of one out of four water molecules at 379 K, one water molecule at about 623 K, and a little more than one water molecule at 708 K, the latter water loss being associated to a phase change. Alberti

and coworkers studied samples heated and quenched in vacuum conditions, so that their room-temperature experiments are hardly comparable with other experiments performed in air. However they describe the detailed crystal structures of yugawaralite before the reported phase transition containing 8.3, 8.0, and 4.0 water molecules per cell (samples YUGA, YU100, and YU150, respectively), and of yugawaralite after the phase transition containing approximately 4.0 water molecules per cell (samples YU200 and YU250). According to their study the phase transition involves a change in coordination of the Ca cations, which at high temperature strongly interact with five framework O atoms, a remarkable distortion of the tetrahedral framework, the doubling of the a cell parameter (and of course of the cell volume), and the change of space group symmetry from Pc to Pn (Alberti et al. 1994, 1996).

The present study is part of a systematic investigation of the structural response of natural zeolites to temperature-induced dehydration (see Ståhl 1994; Artioli 1999 for reviews), using *in situ* time-resolved powder diffraction and synchrotron radiation. Such experimental conditions are ideal for rapid data collection of diffraction data necessary to follow in detail each step of the dehydration process. Rietveld analysis of the pow-

*E-mail: artioli@iummix.terra.unimi.it

der diffraction data commonly yields a complete and continuous picture of the structure response during the process (see for example: laumontite, Ståhl et al. 1996; stilbite, Cruciani et al. 1997).

SAMPLE PREPARATION

The yugawaralite powder sample used in the present study (Hvalfjörður, Iceland; specimen Ni-6932 of the Icelandic Museum of Natural History, Reykjavik) was prepared by hand grinding a fragment of the large single crystal used for a previous neutron diffraction investigation at low temperature (Kvick et al. 1986). The obvious advantages derived from the sample choice are: (1) the tested chemical and phase purity of the sample, and (2) the availability of an exceptionally well-defined atomic model for the starting crystal structure.

The thermal analysis of the Icelandic sample was performed in air using a NEC instrument and a 5 °/min heating rate. The weight loss curve (Fig. 1) is very similar to the one reported by Gottardi and Galli (1985) for the yugawaralite sample from Sardinia and they both shows the absence of the 927 K shoulder present in the dehydration curve of the sample from Yugawara (Alberti et al. 1996).

The powder sample was loaded and gently compacted in a glass capillary with diameter 0.3 mm, open at both ends.

POWDER DATA COLLECTION AND TREATMENT

Powder diffraction data were collected at beamline X7b of the National Synchrotron Light Source, Brookhaven National Laboratory, U.S.A. The capillary sample was mounted on a standard goniometer head and kept spinning during the data collection in parallel beam Debye geometry, using a Si(111) monochromatized wavelength of 1.488 Å (calibrated against the NBS-640b Si standard, assuming $a = 5.43094(4)$ Å at 298 K). A fixed curved position sensitive detector (CPS120 by INEL, see Ståhl and Hanson 1994 for calibration details) was

used to record the full diffraction pattern using fixed accumulation times. By using a ramp-and-pause mode of sample heating with steps of about 6 K, a total number of 77 powder spectra were collected in the temperature range 315–777 K, each spectrum being collected for about 5 min at constant temperature.

The raw counts versus detector channel data were calibrated in angle using a cubic spline function interpolation of the detector scan performed using the attenuated primary beam (Ståhl and Hanson 1994).

More data of the high-temperature phase were collected by high-resolution powder diffraction using an Image Plate at beamline BM8 of the European Synchrotron Radiation Facility, Grenoble, France. The high-temperature phase was stabilized by heating the sample at 770 K under dry N₂ flux. High-resolution diffraction data of this phase were collected at 770 K and room temperature.

RIETVELD REFINEMENTS: THE STRUCTURE MODELS OF LOW-TEMPERATURE AND HIGH-TEMPERATURE YUGAWARALITE

Spectra were analyzed by Rietveld profile fitting using the GSAS software (Larson and Von Dreele 1998). Bragg peak profiles were modeled by a pseudo-Voigt function corrected for asymmetry with three refinable coefficients. The instrumental background was empirically modeled by a twelve-coefficient Chebyshev polynomial of the first kind. The angular shift was accurately refined in the 315 K pattern, and subsequently kept fixed at the refined value.

The starting atomic coordinates for yugawaralite at 315 K were from the neutron refinement of Kvick et al. (1986), ignoring the hydrogen atom positions. The labels of atoms adopted by Kvick et al. (1986) were retained. The refinement in space group *Pc* [cell parameters: $a = 6.7320(1)$, $b = 14.0157(2)$, $c = 10.0607(1)$ Å, $\beta = 111.189(1)^\circ$, $Z = 2$] converged, allowing direct determination of the site occupancy factors of the par-

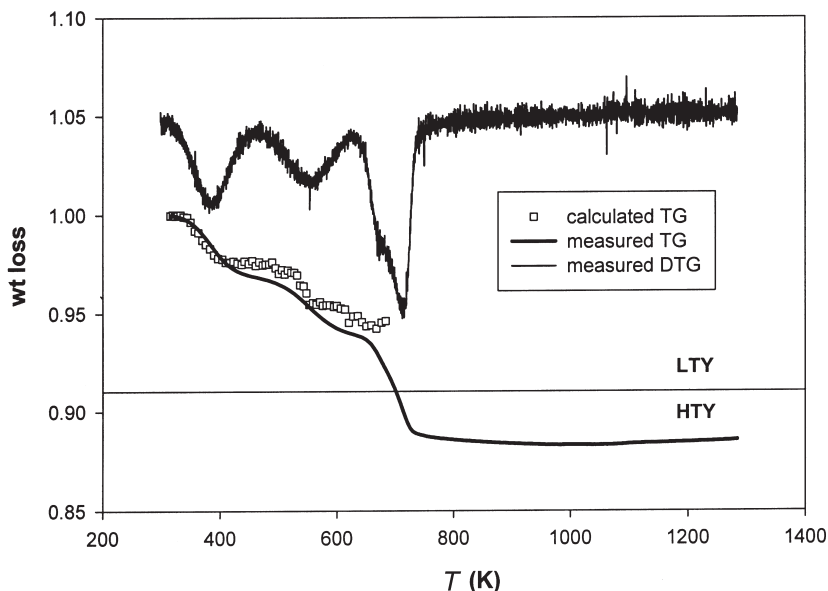


FIGURE 1. Thermogravimetric curves of yugawaralite from Iceland. Thick line is the measured weight loss percent, thin line is the measured differential curve, open squares show the weight loss calculated from the refined occupancies of the water sites of the low-temperature yugawaralite phase (see text for details).

tially occupied water sites (OW1-OW1a, OW4-OW4a, OW5), and confirmation that the water sites OW2 and OW3 are fully occupied at room temperature. The total amount of water molecules obtained from the refinement (8.6 water molecules/cell) is slightly higher than that obtained from the neutron refinement, due to the higher site occupancy factor observed for OW5, that is the water molecule not connected to Ca cations. The effect may be related to the different water partial pressure on the sample in the two experiments: sealing and cooling of the yugawaralite crystal under N_2 atmosphere for the neutron experiment may have caused slight dehydration of the sample. The site distribution of the water molecules in the two split water sites (OW1, OW4) results to be very similar: 0.86:0.14 for the OW1:OW1a sites, and 0.88:0.12 for the OW4:OW4a sites. In both instances, the combined sites are fully occupied at room temperature, in agreement with previous refinements (Kvick et al. 1986, Alberti et al. 1996).

In the final cycles the following parameters were simultaneously refined: one scale factor, the unit-cell parameters, the peak profile and background function coefficients, the atomic coordinates, four isotropic displacement parameters (one each for the tetrahedral Si,Al cations, the framework O atoms, the Ca cation, and the water O atoms), and the site occupancy factors of the partially occupied water sites. The results of the 315 K refinements were used as input for the refinement at the next temperature, and the structure of the low-temperature yugawaralite (LTY) was successfully refined for all data sets in the range 315–620 K. Final observed and calculated powder patterns for this phase at 315, 454, and 581 K are shown in Figures 2a to 2c. Refinement parameters are reported in Table 1 and the refined atomic coordinates in Table 2.

The Bragg peaks of the high-temperature phase first appear in the 627 K powder pattern, and the two phases coexist up to 708 K. Above this temperature high-temperature yugawaralite (HTY) alone is present. The relative proportions of the two phases (LTY:HTY) resulting from the refined Rietveld scale factors are: 90:10 at 676 K, 75:25 at 689 K, 58:42 at 695 K, 10:90 at 701 K, and 5:95 at 708 K.

Although no kinetic analysis of the data was performed, the appearance and presence of sharp independent Bragg peaks for HTY, rather than broadening and splitting of the LTY diffraction peaks (none of such features is actually observed), indicates that the observed phase transition in the range 620–708

TABLE 1. Rietveld refinement parameters for yugawaralite

Temperature (K)	315	454	581	749
Space group	Pc	Pc	Pc	Pn
a (Å)	6.73200(9)	6.75075(9)	6.7836(1)	12.703(1)
b (Å)	14.0157(2)	14.0285(2)	13.9842(2)	13.067(1)
c (Å)	10.0607(1)	10.0289(1)	10.0736(2)	9.839(7)
β (°)	111.189(1)	111.216(1)	111.443(1)	110.894(9)
Cell volume (Å ³)	885.09(2)	885.39(2)	889.47(2)	1525.8(1)
R_p	0.057	0.058	0.054	0.062
R_{wp}	0.074	0.074	0.070	0.081
R_{F2}	0.075	0.076	0.074	0.164
χ^2	5.33	4.21	3.10	5.66
no. of variables	122	117	119	187
no. of observations	3703	3701	3704	3961
no. of reflections	1536	1537	1537	2745

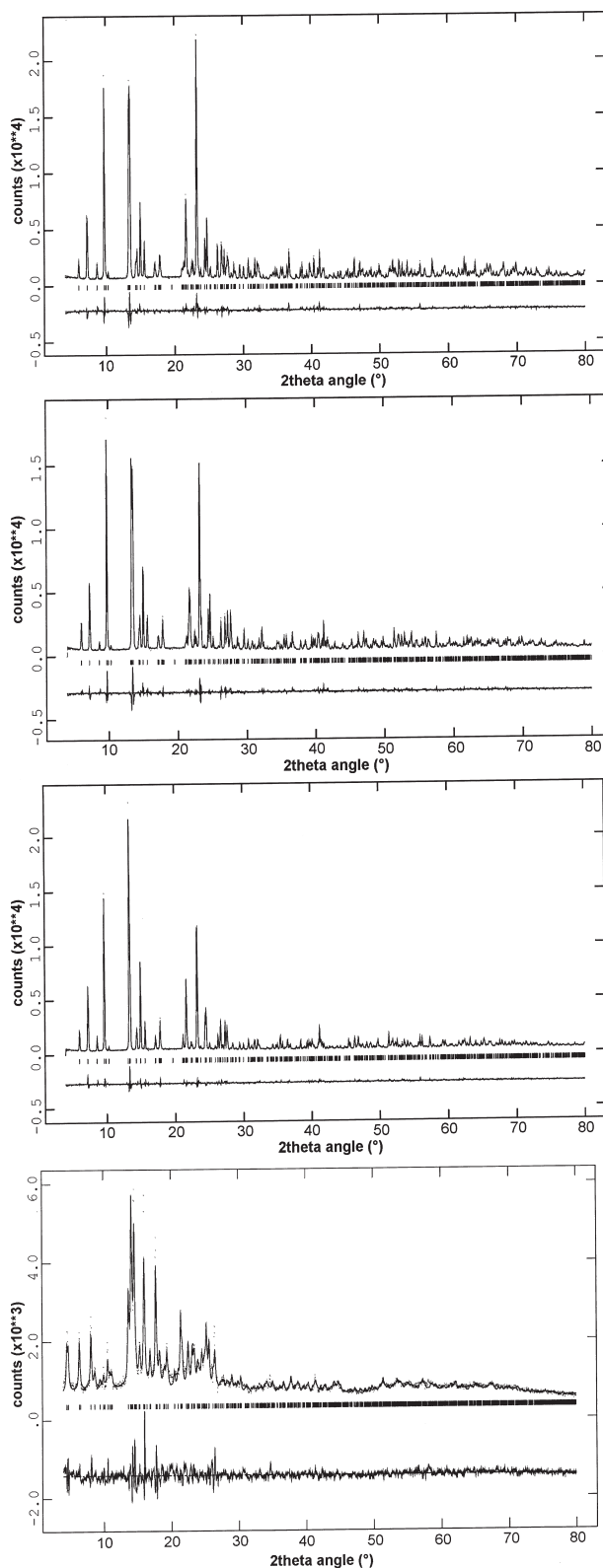


FIGURE 2. Observed (dotted upper line), calculated (solid upper line), and difference (solid lower line) powder diffraction patterns of low-temperature yugawaralite at 315 (a), 454 (b), 581 K (c), and of high-temperature yugawaralite at 749 K (d).

TABLE 2. Refined atomic coordinates for low temperature yugawaralite at 315, 454, and 581 K

T(K)	Atom	x	y	z	Occ.	U_{iso}
315	Si1	0.338(2)	0.1498(6)	0.984(1)	1	0.0049(5)
454	Si1	0.336(2)	0.1480(6)	0.980(1)	1	0.0089(5)
581	Si1	0.337(2)	0.1503(7)	0.986(1)	1	0.0168(6)
315	Si2	0.704(2)	0.0352(5)	0.192(1)	1	0.0049(5)
454	Si2	0.706(2)	0.0353(6)	0.190(1)	1	0.0089(5)
581	Si2	0.707(2)	0.0324(7)	0.194(1)	1	0.0168(6)
315	Si3	0.407(1)	0.1250(6)	0.697(1)	1	0.0049(5)
454	Si3	0.408(1)	0.1281(6)	0.690(1)	1	0.0089(5)
581	Si3	0.405(2)	0.1267(7)	0.694(1)	1	0.0168(6)
315	Si4	0.019(2)	0.4750(5)	0.438(1)	1	0.0049(5)
454	Si4	0.019(2)	0.4764(6)	0.440(1)	1	0.0089(5)
581	Si4	0.021(2)	0.4717(6)	0.462(1)	1	0.0168(6)
315	Si5	0.354(2)	0.3718(6)	0.962(1)	1	0.0049(5)
454	Si5	0.353(2)	0.3715(6)	0.961(1)	1	0.0089(5)
581	Si5	0.357(2)	0.3693(7)	0.965(1)	1	0.0168(6)
315	Si6	0.736(1)	0.5005(5)	0.6260(9)	1	0.0049(5)
454	Si6	0.730(1)	0.5034(5)	0.6232(9)	1	0.0089(5)
581	Si6	0.730(2)	0.5056(6)	0.645(1)	1	0.0168(6)
315	AL1	0	0.0062(5)	0	1	0.0049(5)
454	AL1	0	0.0036(5)	0	1	0.0089(5)
581	AL1	0	-0.0022(7)	0	1	0.0168(6)
315	AL2	0.389(2)	0.3555(6)	0.652(1)	1	0.0049(5)
454	AL2	0.381(2)	0.3541(6)	0.647(1)	1	0.0089(5)
581	AL2	0.385(2)	0.3548(7)	0.652(1)	1	0.0168(6)
315	O1	0.102(2)	0.1053(9)	0.943(2)	1	0.007(1)
454	O1	0.103(2)	0.103(1)	0.946(2)	1	0.015(1)
581	O1	0.112(3)	0.101(1)	0.965(2)	1	0.027(1)
315	O2	0.848(3)	0.046(1)	0.095(2)	1	0.007(1)
454	O2	0.853(3)	0.050(1)	0.096(2)	1	0.015(1)
581	O2	0.835(3)	0.034(1)	0.087(2)	1	0.027(1)
315	O3	0.187(2)	0.078(1)	0.593(2)	1	0.007(1)
454	O3	0.192(2)	0.080(1)	0.585(2)	1	0.015(1)
581	O3	0.172(2)	0.092(1)	0.593(2)	1	0.027(1)
315	O4	0.514(2)	0.113(1)	0.133(1)	1	0.007(1)
454	O4	0.516(2)	0.112(1)	0.127(2)	1	0.015(1)
581	O4	0.531(3)	0.114(1)	0.126(2)	1	0.027(1)
315	O5	0.429(3)	0.125(1)	0.861(1)	1	0.007(1)
454	O5	0.422(3)	0.128(1)	0.853(1)	1	0.015(1)
581	O5	0.414(3)	0.132(2)	0.855(2)	1	0.027(1)
315	O6	0.615(2)	0.0730(8)	0.687(2)	1	0.007(1)
454	O6	0.608(3)	0.0713(8)	0.677(2)	1	0.015(1)
581	O6	0.611(3)	0.0743(9)	0.683(2)	1	0.027(1)
315	O7	0.853(2)	0.0613(9)	0.353(1)	1	0.007(1)
454	O7	0.848(3)	0.0635(9)	0.353(1)	1	0.015(1)
581	O7	0.874(3)	0.067(1)	0.346(1)	1	0.027(1)
315	O8	0.334(3)	0.2634(5)	0.008(2)	1	0.007(1)
454	O8	0.325(4)	0.2620(5)	-0.001(2)	1	0.015(1)
581	O8	0.330(4)	0.2632(6)	0.019(2)	1	0.027(1)
315	O9	0.408(3)	0.2329(6)	0.643(2)	1	0.007(1)
454	O9	0.401(3)	0.2328(6)	0.623(2)	1	0.015(1)
581	O9	0.425(3)	0.2333(7)	0.640(2)	1	0.027(1)
315	O10	0.159(2)	0.4283(9)	0.986(2)	1	0.007(1)
454	O10	0.158(2)	0.4268(9)	0.984(2)	1	0.015(1)
581	O10	0.175(3)	0.437(1)	0.983(3)	1	0.027(1)
315	O11	0.832(2)	0.482(1)	0.502(2)	1	0.007(1)
454	O11	0.828(2)	0.486(1)	0.500(2)	1	0.015(1)
581	O11	0.845(3)	0.492(1)	0.532(2)	1	0.027(1)
315	O12	0.162(2)	0.3808(8)	0.503(2)	1	0.007(1)
454	O12	0.149(2)	0.3798(8)	0.504(2)	1	0.015(1)
581	O12	0.157(3)	0.3741(9)	0.504(2)	1	0.027(1)
315	O13	0.576(2)	0.4086(9)	0.082(2)	1	0.007(1)
454	O13	0.579(2)	0.4038(9)	0.079(2)	1	0.015(1)
581	O13	0.567(3)	0.405(1)	0.093(2)	1	0.027(1)
315	O14	0.360(3)	0.392(1)	0.807(1)	1	0.007(1)
454	O14	0.360(3)	0.390(1)	0.805(1)	1	0.015(1)
581	O14	0.364(4)	0.391(1)	0.811(2)	1	0.027(1)
315	O15	0.624(2)	0.4022(8)	0.645(2)	1	0.007(1)
454	O15	0.605(2)	0.4072(9)	0.634(2)	1	0.015(1)
581	O15	0.611(3)	0.405(1)	0.639(2)	1	0.027(1)
315	O16	0.935(2)	0.467(1)	0.266(1)	1	0.007(1)
454	O16	0.918(2)	0.462(1)	0.268(1)	1	0.015(1)
581	O16	0.902(3)	0.456(1)	0.293(1)	1	0.027(1)
315	CA	0.041(1)	0.2169(4)	0.424(1)	1	0.012(2)
454	CA	0.011(2)	0.2214(5)	0.445(1)	1	0.026(2)
581	CA	0.034(2)	0.2224(5)	0.434(1)	1	0.033(2)
315	OW1	0.985(5)	0.250(1)	0.177(3)	0.86(7)0.020(3)	

TABLE 2—Continued

T(K)	Atom	x	y	z	Occ.	U_{iso}
454	OW1	0.059(4)	0.235(2)	0.219(2)0.99(3)	0.059(5)	
581	OW1	0.060(5)	0.242(2)	0.202(4)	1	0.128(9)
315	OW1A	0.04(3)	0.29(2)	0.21(2)	0.14(7)0.020(3)	
454*	OW1A	0.0050	0.3430	0.1970	0.01(3)0.059(5)	
581	OW1A	—	—	—	—	
315	OW2	0.897(3)	0.234(1)	0.620(2)	1	0.020(3)
454	OW2	0.867(3)	0.231(2)	0.618(2)	1	0.059(5)
581	OW2	0.814(5)	0.235(3)	0.557(4)	1	0.128(9)
315	OW3	0.676(3)	0.284(1)	0.334(2)	1	0.020(3)
454	OW3	0.664(4)	0.281(2)	0.331(2)	1	0.059(5)
581	OW3	0.674(8)	0.264(5)	0.374(6)0.53(4)	0.128(9)	
315	OW4	0.341(4)	0.150(2)	0.351(4)0.88(8)	0.020(3)	
454*	OW4	0.3050	0.1520	0.330	0.11(4)	0.059(5)
581	OW4	—	—	—	—	
315	OW4A	0.32(3)	0.13(1)	0.28(3)	0.12(8)	0.020(3)
454	OW4A	0.33(2)	0.087(9)	0.30(1)	0.20(3)	0.059(5)
581	OW4A	0.33(2)	0.100(7)	0.27(1)	0.31(3)	0.128(9)
315	OW5	0.793(9)	0.259(5)	0.912(6)0.29(2)	0.020(3)	
454	OW5	0.835(9)	0.231(4)	0.954(5)0.38(3)	0.059(5)	
581	OW5	0.87(2)	0.22(1)	0.99(1)	0.23(4)	0.128(9)

* Coordinates not refined.

K is a true first order transformation, probably involving nucleation and growth of the high-temperature phase, rather than a simple distortion of the low-temperature structure.

Extensive modeling was performed on the 749 K data set containing the HTY alone, and on the comparable data sets collected at ESRF, to derive an acceptable structure model for this phase. The structure model proposed by Alberti et al. (1996: samples YU200 and YU250), involving a cell doubling along *a* with space group *Pn*, although refinable to a certain degree, could not satisfactorily model the features observed in the powder patterns. The following observations indicate that the proposed model is at best an approximate structure model of the high-temperature phase, and that the true structure must have a larger unit cell and a more complex structure. (1) First, several observed Bragg peaks are completely unaccounted for by the doubled *Pn* unit cell (Fig. 3). (2) Second, the tetrahedral framework geometry could not be fully refined, even by imposing severe constraints on the T-O and T-T bond distances. (3) Third, the occupancy factors of the two independent Ca sites were heavily correlated, possibly indicating that the two positions are symmetry related, and resulting in chemically unreasonable cell cation content. Finally (4) no water molecule position could be possibly located either in the difference Fourier maps or by tentative refinement of the originally proposed water oxygen positions.

The following alternative structure models were tentatively optimized by distance least squares modeling, and then tested by Rietveld refinement. (1) The first one is a structure model having a unit cell doubled along *c* with respect to LTY, and space group *Pn*. (2) The second one is a structure model having a unit cell doubled along *c* with respect to LTY, and space group *Pa*. (3) The third one is a structure model having a unit cell doubled along *b* with respect to LTY, and space group *Aa*. (4) The fourth one is a structure model having a unit cell doubled both along *a* and *c* with respect to LTY, and space group *Pn* or *Pa*. (5) The fifth model is a structure model having a unit cell doubled both along *a* and *b* with respect to LTY, and space group *Cc* or *Cn*. (6) The final model is a structure model having a unit cell doubled along all three directions with respect to

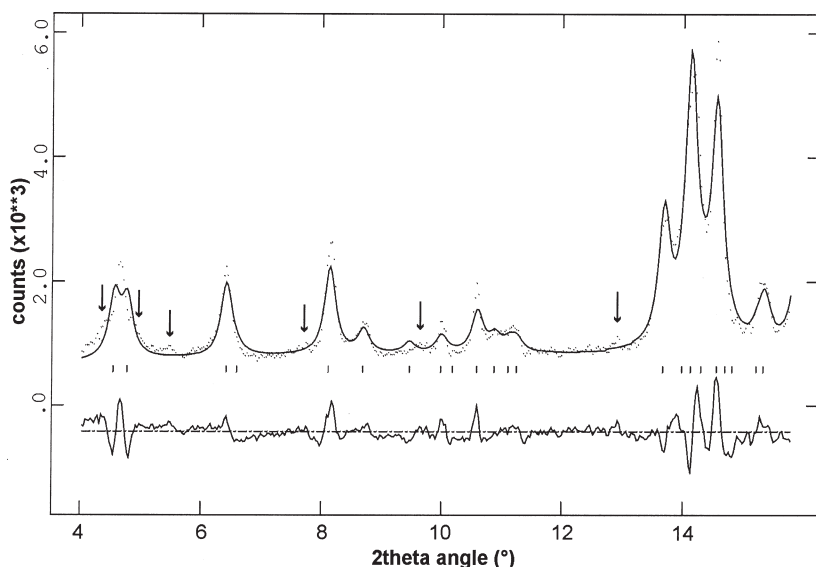


FIGURE 3. Portion of the low-angle powder pattern of high-temperature yugawaralite at 749 K, showing the discrepancy between the observed data and the calculated profile using the structure model proposed by Alberti et al. (1996). The arrows indicate observed Bragg peaks which are not taken into account by the model.

LTY, and space group *Aa*.

None of the models having a cell volume doubled with respect to LTY (i.e., models 1–3 above) could produce a satisfactory refinement. The more complex models (i.e., models 4–6 above, involving cell volumes four to eight times the original LTY cell) in addition to unsatisfactory modeling of the observed data, also displayed severe parameter correlation and could not be supported by the powder data.

Despite the effort devoted to structure modeling and pattern simulation, and the fact that the previously proposed model can not fully account for the observed data, no proper model for the high-temperature phase can be proposed at this stage. For the time being, we assumed the average structure model proposed by Alberti et al. (1996, Yu200 sample) by keeping the atomic coordinates fixed at the literature values, and used this approximate model of the HTY structure to extract the temperature dependence of its unit-cell parameters, and the relative phase proportions of the two phases over the temperature range 627–777 K. Observed and calculated powder diffraction patterns of HTY at 749 K are shown in Figure 2d. Refinement parameters are in Table 1.

THE DEHYDRATION PROCESS: RESULTS AND DISCUSSION

The first-order phase transition between the two phases present in the temperature range 680–720 is accompanied by a large decrease in the cell volume (Fig. 4). The transition temperature will be arbitrarily assumed at 695 K, because at this temperature the two phases have nearly equal proportions. Of course, the transition temperature depends on the heating rate and other environmental conditions.

In HTY, all cell parameters continuously and smoothly decrease and no significant changes are present. Although complete refinement of the high-temperature structure was not possible, the trend in the cell volume indicates a gradual and continuous release of water molecules, with no abrupt structural changes.

In LTY, the temperature dependence of the cell volume

shows at least three distinct regions: (1) a small decrease in the temperature range 340–390 K; (2) an almost linear substantial increase in the temperature range 390–500 K; and (3) a small increase in the temperature range 500–680 K. The three dehydration steps are reflected in the temperature behavior of the unit-cell parameters (Fig. 4) and in the content of water molecules in the zeolite channels (Fig. 5a). The different dehydration steps perfectly correspond to the broad exothermal peaks present in the differential thermal curve, and the weight loss curve calculated from the refined occupancy parameters of the water molecules is in very good agreement with the measured curve (Fig. 1).

The following detailed discussion of the dehydration process can be visualized by referring to Figure 3 of Kvik et al. (1986), atom labels are the same.

The structure of low-temperature yugawaralite shows no changes up to 340 K, where the first dehydration step occurs. This step, occurring between 340 and 390 K, is essentially related to the variation of the occupancy factors of the split water molecules (OW1, OW4), as shown in Figure 6. The site occupancy factor of OW1a neatly decreases and OW1a is essentially empty above 360 K; the water molecules located in this position are not released, but shifted to the main OW1 site, which is then fully occupied above this temperature. In contrast, the low occupancy OW4a site has an essentially constant occupancy factor (~0.2) up to 500 K, and it is not affected by this early dehydration step; whereas the main OW4 site shows a neat and continuous decrease in the occupancy factor (from 0.80 at 337 K to 0.15 at 396 K), which is the main cause of the general decrease in water content (Fig. 5) and in volume (Fig. 4) in this temperature range. Part of the water molecules expelled from the OW4 water site are diffusing in the OW5 site, which shows a partial and sharp rehydration at this stage. The same effect, involving release of cation-bonded water molecules and concomitant occupation of only hydrogen-bonded sites, was observed in laumontite (Ståhl et al. 1996).

Water is not expelled completely from the combined OW4

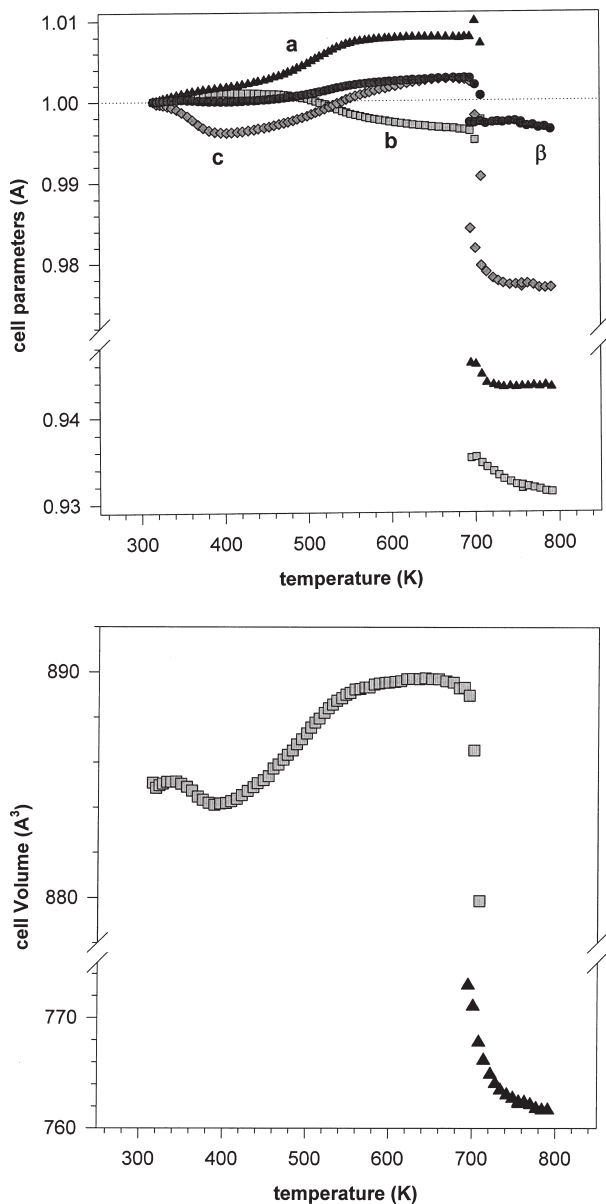


FIGURE 4. Temperature dependence of the unit-cell parameters (angstroms and degrees) and of the volume (\AA^3) of low-temperature (open squares) and high-temperature (solid triangles) yugawaralite. The values of the unit-cell parameter a and of the volume of high-temperature yugawaralite have been halved for comparison with LTY.

sites (Figs. 5b and 6), and both OW4 and OW4a retain a constant and similar occupancy level (close to 0.15) during the second dehydration step. No water at all is released from the channels in the temperature range 390–494 K, and the variation of the volume and the cell parameters in this temperature range are only affected by thermal expansion. The coordination of the Ca cation at this stage is 4 framework O atoms and $3.3 \text{ H}_2\text{O}$.

At 494 K, the occupancy factor of the OW3 site starts to

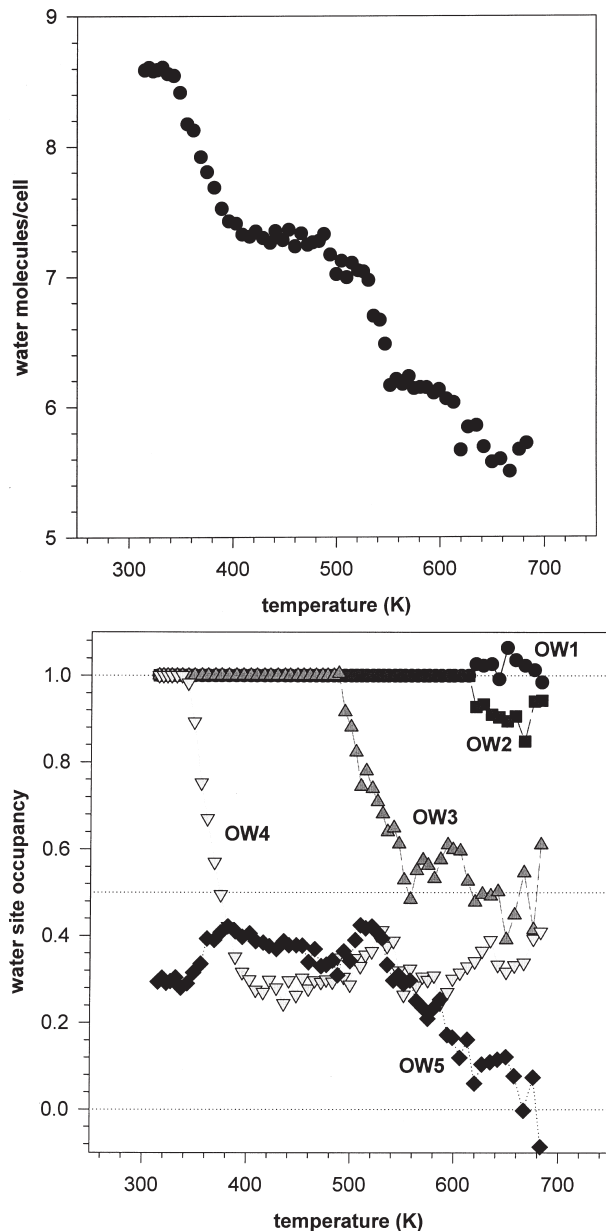


FIGURE 5. Water content of low-temperature yugawaralite as a function of temperature: (a) total amount of water molecules per cell; (b) site occupancies of the crystallographic water sites (●:OW1, ■:OW2, ▲:OW3, ▼:OW4, ◆:OW5). The combined occupancy of the split OW1 and OW4 water sites are reported. Individual occupancies of each site are shown in Figure 5.

decrease, and in the early part of the third dehydration step there is continuous decrease from 1.0 at 488 K to 0.5 at 552 K, despite the fact that there is very little change in the thermal expansion regime in the cell volume or in the other cell parameters (Fig. 4). At the same temperature the occupancy of the OW4 site drops to 0 while that of the OW4a site increases to 0.3. No split water sites are present above 530 K (Fig. 6). At 530 K the Ca cations are still effectively sevenfold-coordinated to four framework O atoms and three water oxygen atoms (the

fully occupied OW1 and OW2, and the partially occupied OW3 and OW4 sites, at the 0.7 and 0.3 level respectively). At about 530 K the water molecules located in the OW5 site also start to diffuse out of the channels, and the site is effectively empty at 620 K. Between 500 and 620 K water molecules are continuously released from LTY, with both OW3 and OW5 contributing differently to the process (Fig. 5a): the maximum rate of dehydration is observed in the 520–550 K temperature range when water molecules are simultaneously released from both sites.

Between 530 and 680 K, the Ca cations in LTY essentially maintain a sevenfold- coordination, as the Ca-bonded water molecules (OW1, OW2, OW3, OW4) have an almost constant occupancy level in the 530–680 K temperature range, that is up to the structural phase transition. Because some water is released from the sample at this stage according to the thermal gravimetric analysis, and the H-bonded water site OW5 is empty, the dehydration process implies that the released water molecules from LTY above 620 K are Ca-bonded and that at the same time the phase transition to the low-water content HTY takes place. Correspondingly, the peaks of the high-temperature phase appear in the powder pattern at this temperature.

The major 695 K phase transition is therefore driven by the Ca cation rearrangement: apparently there is no possibility of shifting to 6-coordination of the Ca atoms in the LTY structure, and as soon as the coordination falls below 7 (i.e., when the number of bonded water molecules falls below 3) the Ca atoms increase their coordination by forming new bonds with

framework O atoms. The same mechanism has been observed in other Ca-rich zeolites (laumontite, scolecite, mesolite: Ståhl and Hanson 1994; Artioli 1999), although this rearrangement usually occurs when the coordination of the Ca atoms falls below 6. The higher limit for the Ca geometry observed in LTY may be due to the relative rigidity of the yugawaralite framework. The major phase transition is well recorded in the thermogravimetric curve as a large exothermal peak at 690 K (Fig. 1).

According to the proposed model for the structure of high-temperature yugawaralite (Alberti et al. 1996), the Ca cations in HTY are bonded to five framework O atoms and one water molecule. The change in Ca coordination drastically distorts the framework topology and it is observed in the dramatic change in the cell parameters at the transition.

The influence of the release of each water molecule on the change of the cell volume of LTY is evaluated from Figure 7. In the first dehydration step, the release of the OW4 water molecule negatively affects the volume, largely overcoming the effect of lattice thermal expansion. The large increase in volume from 884 to 889 Å³ is caused by thermal expansion alone, as almost no water is released at this stage. Then the release of the OW3 and OW5 water molecules is again effectively counterbalancing the volume thermal expansion, although its effect is much smaller than the one caused by the release of OW4. The cell volume still expands during the release of OW3 and OW5, but at a much smaller rate.

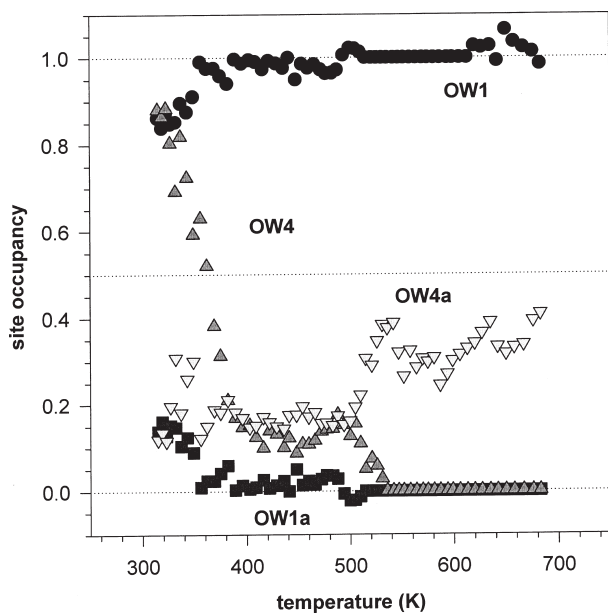


FIGURE 6. Site occupancy factors of the split OW1, OW4 water sites as a function of temperature. The site occupancy factor of OW1 was fixed to 1.0 above 515 K.

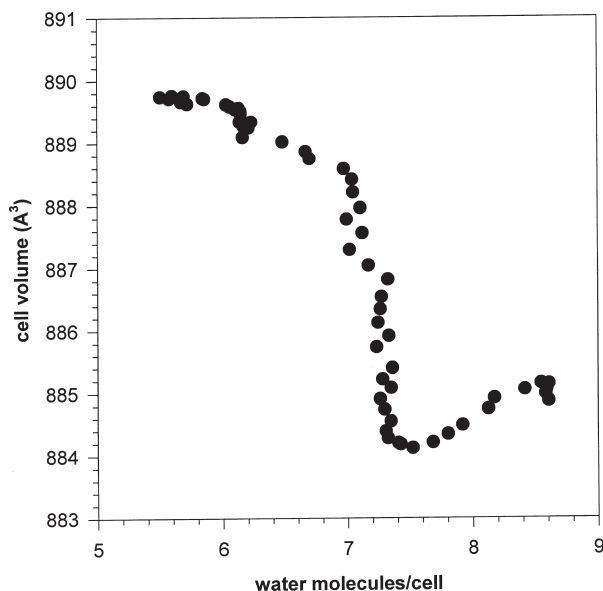


FIGURE 7. Dependence of the cell volume from the total water content in yugawaralite.

ACKNOWLEDGMENT

G.A., G.C., and A.G. thank Italian MURST and CNR and K.S. thanks the Swedish NFR for financial assistance. The synchrotron powder data collections were carried out at Brookhaven National Laboratory and supported under contract DE-AC02-98CH10886 with the U.S. DOE by its Division of Chemical Sciences, Office of Basic and Energy Sciences. S.P. Jakobsson kindly provided the yugawaralite crystals. C. Cristiani kindly performed the thermal analyses.

REFERENCES CITED

- Alberti, A., Quartieri, S., and Vezzalini, G. (1994) Structural modifications induced by dehydration in yugawaralite. *Studies in Surface Science and Catalysis*, 84, 637–644.
- Alberti, A., Quartieri, S., and Vezzalini, G. (1996) Thermal behaviour of zeolites: single crystal X-ray study of dehydration and rehydration mechanism in yugawaralite. *European Journal of Mineralogy*, 8, 1273–1282.
- Artioli, G. (1999) In situ structural and kinetic powder diffraction studies of aluminosilicates. In K. Wright and R. Catlow, Eds., *Microscopic properties and processes in minerals*, NATO Science Series, Series C, 543, 177–187. Kluwer, Dordrecht, The Netherlands.
- Cruciani, G., Artioli, G., Gualtieri, A., Ståhl, K., and Hanson, J.C. (1997) Dehydration dynamics of stilbite using synchrotron X-ray powder diffraction. *American Mineralogist*, 82, 729–739.
- Eberlein, G.D., Erd, R.C., Weber, F., and Beatty, L.B. (1971) New occurrence of yugawaralite from the Chena Hot Springs Area, Alaska. *American Mineralogist*, 56, 1699–1717.
- Gottardi, G. and Galli, E. (1985) *Natural Zeolites*. Springer-Verlag, Berlin.
- Kerr, I.S. and Williams, D.J. (1967) The crystal structure of yugawaralite. *Zeitschrift für Kristallographie*, 125, 220–225.
- Kerr, I.S. and Williams, D.J. (1969) The crystal structure of yugawaralite. *Acta Crystallographica*, B25, 1183–1190.
- Kvick, Å., Artioli, G., and Smith, J.V. (1986) Neutron diffraction study of the zeolite yugawaralite at 13 K. *Zeitschrift für Kristallographie*, 174, 265–281.
- Larson, A.C. and Von Dreele, R.B. (1998) GSAS. General Structure Analysis System. Report LAUR 86–748. Los Alamos National Laboratory, Los Alamos, New Mexico.
- Leimer, H.W. and Slaughter, M. (1969) The determination and refinement of the crystal structure of yugawaralite. *Zeitschrift für Kristallographie*, 130, 99–111.
- Meier, W.M., Olson, D.H., and Baerlocher, Ch. (1996) *Atlas of zeolite structure types*. 4th revised edition. Elsevier, London.
- Ståhl, K. (1994) Real-time powder diffraction studies of zeolite dehydration processes. *Materials Science Forum*, 166-169, 571–576.
- Ståhl, K. and Hanson, J.C. (1994) Real-time X-ray synchrotron powder diffraction studies of the dehydration processes in scolecite and mesolite. *Journal of Applied Crystallography*, 27, 543–550.
- Ståhl, K., Artioli, G., and Hanson, J.C. (1996) The dehydration process in the zeolite laumontite: a real-time synchrotron X-ray powder diffraction study. *Physics and Chemistry of Minerals*, 23, 328–336.
- Tschermich, R.W. (1992) *Zeolites of the world*. Geoscience Press Inc., Phoenix, Arizona.

MANUSCRIPT RECEIVED JANUARY 24, 2000

MANUSCRIPT ACCEPTED AUGUST 14, 2000

PAPER HANDLED BY JAMES W. DOWNS